Microporous and Mesoporous Materials 162 (2012) 91–97

Contents lists available at SciVerse ScienceDirect

Microporous and Mesoporous Materials

journal homepage: www.elsevier.com/locate/micromeso

CO_2 adsorption studies on Prussian blue analogues

F. Karadas [a], H. El-Faki [a], E. Deniz [a], C.T. Yavuz [b,*], S. Aparicio [c,*], M. Atilhan [a,*]

[a] Department of Chemical Engineering, Qatar University, 2713 Doha, Qatar
[b] Graduate School of EEWS, KAIST, 373−1 Guseong Dong, Yuseong Gu, Daejeon 305-701, Republic of Korea
[c] Department of Chemistry, University of Burgos, 09001 Burgos, Spain

ARTICLE INFO

Article history:
Received 30 May 2012
Received in revised form 11 June 2012
Accepted 12 June 2012
Available online 25 June 2012

Keywords:
Prussian blue analogues
Carbon dioxide
Adsorption
High pressure
Monte Carlo

ABSTRACT

Carbon dioxide (CO_2) adsorption capacities of several Prussian blue (PB) analogues have been studied using the state-of-the-art Rubotherm® sorption apparatus to obtain adsorption and desorption isotherms of these compounds up to 50 bar. The analogues were prepared by simply reacting a $[M(CN)_6]^{3-}$ (M=Co, Fe) solution with solutions of M^{2+} (M=Mn, Fe, Co, Ni, Cu) metal ions. Characterization of the studied samples has been performed by using a combination of powder XRD, TGA, FTIR, and CHN elemental analysis. Adsorption capacities of PB analogues calculated with theoretical calculations, using Monte Carlo approach, have also been compared with the experimental study, and used to discuss the molecular mechanism of adsorption.

1. Introduction

Prussian blue (PB) and its analogues have widely been studied due to their fascinating catalytic, photophysical, electronic, and magnetic properties [1–6]. Prussian blue analogues represent a large family of compounds based on a cubic $M'[M(CN)_6]$ framework. One of the remarkable structural properties of PB analogues is that they all exist in the same cubic structure even when metal ions with different oxidation states are used [7,8] The framework, thus, provides its charge balance by creating vacancies, which are filled by H_2O molecules. Considering that vacancies are present in almost one quarter of the $Fe(CN_6)^{4-}$ sites of Prussian blue, such voids could be of significant potential use for gas adsorption since H_2O molecules in these vacancies can be removed under vacuum. Therefore, the number of vacancies could be controlled by choosing the metal ions conveniently. For example, $Mn^{3+}/[Cr(CN)_6]^{3-}$ and $Mn^{3+}/[V(CN)_6]^{3-}$ based compounds do not possess any water molecules since no vacancies are needed to provide the charge balance. However, $Mn^{3+}/[Ni(CN)_6]^{4-}$ ($x = 12$), $Cr^{3+}/[Ni(CN)_6]^{4-}$ ($x = 9$), and $Mn^{2+}/[Mn(CN)_6]^{3-}$ ($x = 12$) based PB analogues have about 10 water molecules per unit cell (x represents the number of water molecules per unit cell) [9]. Recently, these analogues have been studied for adsorption studies due to their microporous behavior. Long et al. observed that dehydrated PB compounds, $M_3[Co(CN)_6]_2$ (M=Mn, Fe, Co, Ni, Cu, Zn), show significant hydrogen sorption at 77 K and 890 Torr, varying from 1.4 wt% and 0.018 kg H_2/L for $Zn_3[Co(CN)_6]_2$ to 1.8 wt% and 0.025 kg H_2/L for $Cu_3[Co(CN)_6]_2$ [10]. CO_2 adsorption studies of $M_3[Co(CN)_6]_2{\cdot}nH_2O$ (M=Co, Zn) were performed by Thallapally et al. [11]. These materials adsorbed 8–10 wt% of CO_2 at room temperature and 1 bar of pressure. Furthermore, these materials adsorbed approximately 20–30 wt% of CO_2 at high pressures (30 bar and 298 K).

In this work, metal ions have been reacted with hexacyanometallates systematically to synthesize a series of PB compounds. Finally, the CO_2 adsorption capacity of these samples will be measured using magnetic suspension sorption device, and molecular simulations using Monte Carlo method will be used to analyze CO_2 adsorption from a nanoscopic viewpoint.

2. Experimental section

2.1. Synthesis

PB analogues are abbreviated as [M3M′2] throughout the text. In a typical procedure, 3 mmol of $K_3[M(CN)_6]$ (M being Fe or Co) was mixed with 3 mmol of MCl_2 (M being Mn, Fe, Co, Ni, Cu, Zn) in 30 mL of aqueous solution for one day. The resulting precipitate was aged, filtered, washed, and dried in air. The products ($[M_3Co_2]$ and $[M_3Fe_2]$) were finally dried at 100 °C in an oven for 24 h and stored in glass vials. The yields were 0.55 g (92%) for $[Co_3Fe_2]$, 0.50 g (85%) for $[Mn_3Fe_2]$, 0.42 g (71%) for $[Fe_3Fe_2]$, 0.55 g (92%) for $[Co_3Fe_2]$, 0.51 g (85%) for $[Ni_3Fe_2]$, 0.45 g (73%) for $[Cu_3Fe_2]$, 0.42 g (70%) for $[Mn_3Co_2]$, 0.44 g (74%) for $[Fe_3Co_2]$, 0.34 g (56%)

* Corresponding authors. Tel.: +34 947258062; fax: +34 947258831 (S. Aparicio).
E-mail addresses: yavuz@kaist.ac.kr (C.T. Yavuz), sapar@ubu.es (S. Aparicio), mert.atilhan@qu.edu.qa (M. Atilhan).

1387-1811/$ - see front matter © 2012 Elsevier Inc. All rights reserved.
http://dx.doi.org/10.1016/j.micromeso.2012.06.019

Table 1
Assignment of IR adsorptions (cm^{-1}) of studied materials.

Compound	Molecular formula	H_2O bending	HOH stretch	CN stretch	M–CN stretch
$[Mn_3Fe_2]$	$Mn_3[Fe(CN)_6]_2{\cdot}10H_2O$	3390 3648	1608	2147	417
$[Fe_3Fe_2]$	$Fe_3[Fe(CN)_6]_2{\cdot}4H_2O$	3450	1608	2123	495 594
$[Co_3Fe_2]$	$Co_3[Fe(CN)_6]_2{\cdot}5H_2O$	3418 3632	1603	2127	538
$[Ni_3Fe_2]$	$Ni_3[Fe(CN)_6]_2{\cdot}8H_2O$	3385 3646	1609	2163	420 429
$[Cu_3Fe_2]$	$Cu_3[Fe(CN)_6]_2{\cdot}9H_2O$	3260 3385 3622	1609	2093	483 590
$[Mn_3Co_2]$	$Mn_3[Co(CN)_6]_2{\cdot}9H_2O$	3408	1608	2134	420
$[Fe_3Co_2]$	$Fe_3[Co(CN)_6]_2{\cdot}4H_2O$	3404 3647	1610	2168	443
$[Co_3Co_2]$	$Co_3[Co(CN)_6]_2{\cdot}8H_2O$	3450 3638	1619	2180	457
$[Ni_3Co_2]$	$Ni_3[Co(CN)_6]_2{\cdot}9H_2O$	3375 (b) 3645 (s)	1609	2180	455
$[Cu_3Co_2]$	$Cu_3[Co(CN)_6]_2{\cdot}6H_2O$	3420	1609	2170	460

for $[Co_3Co_2]$, 0.31 g (51%) for $[Ni_3Co_2]$, and 0.35 g (56%) for $[Cu_3Co_2]$.

2.2. Physical measurements

IR spectra were measured as powder samples on a Perkin-Elmer Spectrum 400 FT-IR spectrometer, Table 1. Thermal analysis was performed using a Perkin Elmer Pyris 6 TGA instrument. TGA measurements were made at 10 °C/min from 30 to 600 °C under N_2 on all synthesized samples. The diffraction patterns of powdered samples were recorded using a Bruker D2 X-ray diffractometer at 30 kV and 300 mA. Measurements were performed for 2θ in the range of 5–80° with a step size of 0.01° and scan speed of 2°/min. BET surface area values were obtained with a Micromeritics ASAP 2020 accelerated surface area and porosimetry analyzer at 77 K. Prior to analysis, the samples were degassed at 150 °C for 5 h under vacuum.

2.3. Sorption measurements

For carbon dioxide adsorption measurements, a high-pressure magnetic suspension balance (MSB) sorption device made by Rubotherm Präzisionsmesstechnik GmbH is used. MSB apparatus is rated up to 350 bars at 100 °C and it has two different operation positions. Specifications of the instrument and the experimental procedure have been given elsewhere [12].

Typical measurements start with placing approximate of 0.25 g of sample of interest (that is dried at vacuum and 100 °C for 6 h prior to the adsorption measurement) within the sample holder. First the system is taken under vacuum for 24 h at 60 °C. Carbon dioxide is then pressurized via Teledyne Isco 260D fully automated gas booster and charged into the high-pressure cell, then carbon dioxide adsorption on the sample begin. For each pressure point it takes about 45 min to reach equilibrium (pressure and temperature) and once equilibrium is reached, 4 different set of measurements are taken for a period of 10 min; each data point is collected at every 30 s. The total duration of each temperature and pressure point takes about 50 min. At the end of each pressure point, system goes to next pressure measurement point automatically. In this work, pressure up to 50 bars is used for maximum pressure and at the end of each isotherm, hysteresis check is conducted at each isotherm by collecting desorption data as the system is depressurized.

2.4. Models and simulation

The framework structures of the ten studied Prussian blue (PB) analogues were built from octahedral $[M^{III}(CN)_6]^{3-}$ complexes which are bridged into a simple cubic lattice by M^{2+} ions. All the structures were supposed to be of *Fm3m* crystallographic type, and thus, cubic type unit cells were built according to the experimental powder XRD data. Because of the charge imbalance between the $[M^{III}(CN)_6]^{3-}$ complex and the M^{2+} ions, maintaining charge neutrality in the crystal leads to vacancies for one-third of the M^{3+} sites [13]. Jimenez et al. [14] proposed a non-random vacancy distribution for some PB copper analogues concluding a *Pm3m* space group. Nevertheless, *Fm3m* type structures with randomly distributed vacancies were used along this work for all the studied systems. Water molecules present in vacancies (unsaturated metal centers) can be removed upon heating, and thus, dehydrated systems were used along the simulations. Supercells containing $6 \times 4 \times 4$ unit cells, which were maintained rigid, were used for the simulations.

Lennard–Jones parameters for CO_2 and PB sorbents were obtained from the Universal Force Field (UFF) [15]. Charges for framework atoms were obtained using the QEq method [16], as included in Materials Studio Visualizer [17], whereas for CO_2 molecules $-0.35e$ on the O atoms and $+0.70e$ on the C atom were used [18]. All the used parameters are reported in Table 2. Grand canonical Monte Carlo (GCMC) simulations were carried out at 318 K, with 1×10^7 equilibration steps followed by 1×10^7 production steps to sample the desired thermodynamic properties, for each point calculated at a fixed CO_2 fugacity.

3. Results and discussion

Powder X-ray diffraction analysis revealed that all Prussian blue analogues were isostructural with each other, crystallizing in space group *Fm3m* (Figure S1). The most intense reflections correspond to $2\theta \approx 17°$ (200), $2\theta \approx 24°$ (220), $2\theta \approx 35°$ (400), $2\theta \approx 39°$ (420) and $2\theta \approx 43°$ (422). Bragg reflections of the studied compounds are in agreement with those reported in the literature for related compounds [11]. Therefore, octahedral $[M(CN)_6]^{3-}$ units are linked via octahedrally coordinated, nitrogen-bound M^{2+} ions to give a cubic porous frame-work. Guest H_2O molecules occupy the cavities of the cubic lattice.

The interstitial water molecules can be removed upon heating, leaving the $M[M'(CN)_6]$ framework intact and generating open coordination sites on the metal cation M^{2+}. On moderate heating both coordinated and hydrogen bonded water molecules evolve preserving the material framework. Water content of the compounds has been estimated using the dehydration curves of the TG curves (Table 1). Fig. 1 shows the TG curves for the considered series. The temperature of dehydration follows the order Fe > Co > Ni > Mn > Cu for the $M_3[Fe(CN)_6]_2$ series and Mn > Fe > Ni > Co > Cu for the $M_3[Co(CN)_6]_2$ series indicating that the strength of the electrostatic interaction with H_2O molecules and metal sites in [Cu3M2] analogues is the weakest. FTIR spectroscopy was used mainly to establish the presence of cyanide bonds and water molecules in PB analogues. For all samples, FTIR spectra were collected in the mid-IR range 400–4000 cm^{-1} at ambient temperature and pressure. The stretches tabulated in Table 1 confirm the presence of lattice water at 3650–3350 cm^{-1} (antisymmetric and symmetric O–H stretching modes) and at 1606 cm^{-1} (H–O–H bending mode) and the cyanide bond at 2160 cm^{-1} (CN stretching mode). Likewise, the synthesized compounds should belong to the so-called *insoluble* forms of Prussian blue analogues [19], because of the synthesis procedure, and thus, some of the M^{3+} should occupy some of

Table 2
Lennard-Jones parameters, σ and ε, and partial charges for framework atoms and CO_2 used in this study.

	Fe(II)	Co(II)	Co(III)	Ni(III)	Cu(III)	Mn(III)	Fe(III)	C	N	C(CO_2)	O(CO_2)
σ/Å	2.9120	2.8720	2.8720	2.8340	2.8950	2.9610	2.9120	3.8500	3.6600	3.8510	3.5000
ε/kJ mol^{-1}	0.0544	0.0586	0.0586	0.0628	0.0692	0.0544	0.0544	0.4393	0.2887	0.1050	0.0600
	Co3Fe2	Ni3Fe2	Cu_3Fe_2	Mn_3Fe_2	Fe_3Fe_2	Co_3Co_2	Ni_3Co_2	Cu_3Co_2	Mn_3Co_2	Fe_3Co_2	CO_2
q/e (C)	0.0650	0.0698	0.0500	0.0388	0.0934	0.1075	0.0812	0.0833	0.0912	0.0750	0.7000 (C)
q/e (N)	−0.1951	−0.1673	−0.3000	−0.2120	−0.3699	−0.3378	−0.1641	−0.5220	−0.3735	−0.2291	−0.3500 (N)
q/e (M^{II})	0.5820	0.5100	0.6000	0.5461	0.4800	0.3921	0.5002	0.3018	0.3639	0.4705	
q/e (M^{III})	0.6028	0.5969	0.6500	0.8100	0.5298	0.4982	0.5200	0.7214	0.5510	0.7200	

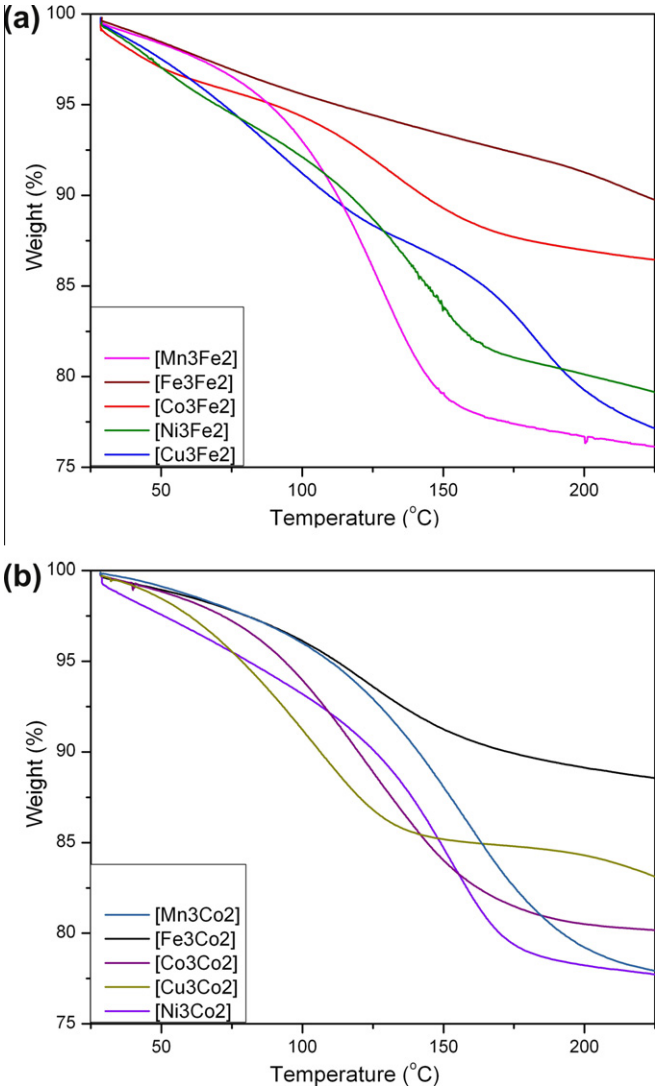

Fig. 1. TG curves of a) $[M_3Fe_2]$ and b) $[M_3Co_2]$ series compounds.

the available interstitial non-framework sites; nevertheless, this occupancy was not tested in this work.

The CO_2 adsorption isotherms in the two families of PB analogues were measured at 318 K up to 50 bar, Figure S2 (Supporting Information). Adsorption–desorption experiments were carried out and no hysteresis was observed. The reported results show moderate CO_2 adsorption abilities in agreement with the microporous character of the studied compounds. For both studied series, compounds containing Cu lead to remarkably larger adsorption abilities in comparison with the other compounds. It should be

Table 3
Accessible surface area, S_{acc} (experimental value in parentheses), and free volume, V_{free}, for the studied PB analogues. Parenthesized values in V_{free} show the percentage of free volume compared with the total volume available (free + occupied).

Compound	S_{acc}/m^2 g^{-1}	V_{free}/cm^3 g^{-1}
$[Co_3Fe_2]$	448 (382)	0.279 (46.4%)
$[Ni_3Fe_2]$	541 (456)	0.305 (47.6%)
$[Cu_3Fe_2]$	422 (502)	0.268 (48.7%)
$[Mn_3Fe_2]$	704 (690)	0.356 (50.2%)
$[Fe_3Fe_2]$	677 (712)	0.342 (49.5%)
$[Co_3Co_2]$	678 (755)	0.370 (54.5%)
	712[a]	
$[Ni_3Co_2]$	670 (534)	0.340 (49.7%)
	560[b]	(58.0%)[d]
	529[c]	
$[Cu_3Co_2]$	689 (760)793[c]	0.369 (53.6%)
$[Mn_3Co_2]$	869 (796)	0.481 (55.3%)
	783[c]	
$[Fe_3Co_2]$	779 (768)	0.373 (51.6%)
	770[b]	

[a] BET surface area from Thallapally et al. [26].
[b] BET surface area from Kaye et al. [10].
[c] BET surface area from Motkuri et al. [27].
[d] Data from Bennet et al. [23].

remarked the very low CO_2 adsorption in $Mn_3[Co(CN)_6]_2$, which is lower than 0.5 mmol g^{-1} in the studied pressure range. Thallapally et al. [11] reported CO_2 adsorption data in $Co_3[Co(CN)_6]_2$, showing 4.8 mmol g^{-1} for CO_2 adsorption at 30 bar and ambient temperature, which is in good agreement with the 3.6 mmol g^{-1} data obtained in this work for the same pressure and 318 K.

The structure of PB analogues is characterized by two types of pores: (i) small pores rising from the defect-free unit cells and (ii) larger pores rising from the random one-third random vacancies because of electrical neutrality. Kaye et al. [10] considered that the unsaturated metal centers present in the large pores are preferential adsorption sites for hydrogen molecules. Natesakhawat et al. [13] reported infrared spectroscopy studies on $M_3[Co(CN)_6]_2$ leading to the conclusion that the differences between the two types of pores do not significantly affect CO_2 adsorption. Nevertheless, considering the very different properties and sizes of the two types of involved pores we have calculated accessible surface area and free volume for the PB analogues studied in this work. The concept of surface areas is controversial in the literature and several definitions have been proposed. Düren et al. [20] proposed the concept of accessible surface area, S_{acc}, to characterize crystalline solids for adsorption purposes, showing clearly better results to compare adsorbents than the commonly used Connolly surface area concept. Accessible surface area is calculated with a probe diameter corresponding to the adsorbate of interest. Therefore, we have used a 3.30 Å probe diameter in this work, corresponding to the kinetic diameter of CO_2 molecules [21]. We have applied the S_{acc} calculation procedure as described by He et al. [22] Calculated free volumes, V_{free}, are obtained from the crystal structures using

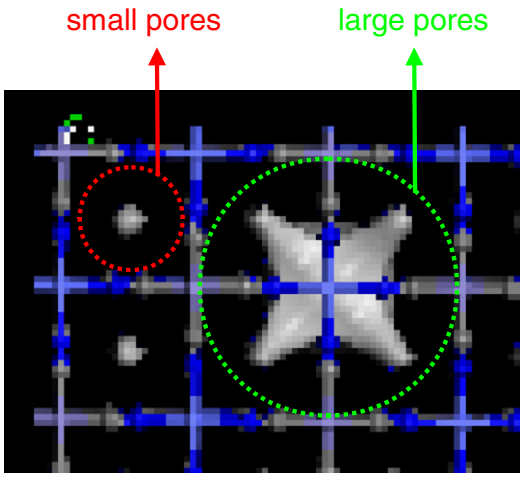

Fig. 2. Free volume in $[Co_3Fe_2]$ showing the differences between small and large pores. The shape of the available volume in large pores should be remarked.

van der Waals radii for framework atoms, and were calculated using a Monte Carlo integration procedure [23]. S_{acc} and V_{free} are reported in Table 3. S_{acc} values are in reasonable agreement with the experimental BET surface area data. For $M_3[Fe(CN)_6]_2$, the ordering of S_{acc} is M = Mn > Fe > Ni > Co > Cu, and the same trend is obtained for V_{free} in agreement with cubic cell parameter a obtained from powder XRD data. For $M_3[Co(CN)_6]_2$, the ordering of S_{acc} is M=Mn > Fe > Cu > Co > Ni (with very small differences between the compounds containing Cu, Co and Ni), whereas the ordering for V_{free} is M=Mn > Fe > Ni > Co > Cu. Therefore, both for $M_3[Fe(CN)_6]_2$ and $M_3[Co(CN)_6]_2$, Mn(II) and Fe(II) lead to the larger S_{acc} and V_{free}, which should contribute to increase adsorption ability for compounds containing these ions.

The obtained S_{acc} and V_{free} are characteristic of microporous materials, nevertheless, the available V_{free} would allow to adsorb remarkable quantities of CO_2 molecules. In spite of the large available V_{free}, there are important differences between the void volume in small and large pore as reported in Fig. 2. The available volume in small pores is only ≈10% of the total available free volume, and thus, from a purely geometrical viewpoint, adsorption in large pores rising from random vacancies would be more suitable, especially for low to moderate pressures.

Using Monte Carlo simulations adsorption isotherms were calculated at 318 K and up to 50 bar pressures and compared with measured data, Fig. 3. A good agreement is obtained between experimental and predicted data, simulations predict correctly the CO_2 adsorption ability ordering of the studied compounds and good quantitative agreement is also obtained, especially for pressures lower than 35 bar. Experimental data show a sudden change for pressures in the 35–40 bar range, which is not predicted by the simulations. These sudden changes may be the consequence of some kind of structural variation in the sorbents crystal structure since the change of the unit cell parameter (a) of PB compounds is observed and studied by several groups at variable temperatures and pressures [24,25]. The sudden changes are not predicted as fixed frameworks have been used for the simulations. Even though there is no literature information on these possible changes at 35–40 bar range in CO_2 media, Thallapally et al. [26] reported experimental CO_2 adsorption data in PB analogues containing Zn and Co up to 30 bar and no sudden changes in the adsorption isotherms were reported. Natesakhawat et al. [13] for Zn and Co containing PB analogues up to 15 bar, and by Motkuri et al. [27] for Cu, Ni and Mn PB analogues up to 30 bar, also did not show any remarkable change in the evolution of CO_2 adsorption isotherms.

The analysis of CO_2 adsorption simulations shows several relevant results. We report in Fig. 4, CO_2 distribution in $Mn_3[Fe(CN)_6]_2$ (the same qualitative behavior is obtained for the remaining PB-based studied sorbents). The isodensity plots show low CO_2 concentrations for the low pressures, and for this initial adsorption stages CO_2 molecules occupy only large pores, with almost null populations in the small pores, Fig. 4a. With increasing pressures, Fig. 2b, large pores are almost fully occupied, and then, CO_2 molecules begin to occupy the available small pores. It should be remarked that the CO_2 distribution in large pores show the same size and shape as the available volume reported in Fig. 4, therefore, showing the importance of the available volume for these microporous sorbents.

Mokturi et al. [27] proposed that the higher the ionic character of the PB-analogues, the higher the CO_2 adsorption, in analogy with the results obtained by Yazaydin et al. [28] for dibenzenedicarboxylate-based metal–organic-frameworks. We have tried to correlate the M^{II}–N and M^{III}–C bond lengths in the crystal models used for the simulations, with the ordering of CO_2 adsorption ability. The experimental ordering for CO_2 adsorption, properly reproduced by simulations, in $M_3[Fe(CN)_6]_2$ is M^{II}=Cu > Co > Mn ~ Ni > Fe, M^{III}–C bond distances follow the ordering M^{III}=Co < Cu < Ni < Fe < Mn. For $M_3[Co(CN)_6]_2$ the CO_2 adsorption ability follows the ordering M^{II}=Cu > Co > Fe > Ni > Mn and the M^{III}–C bond

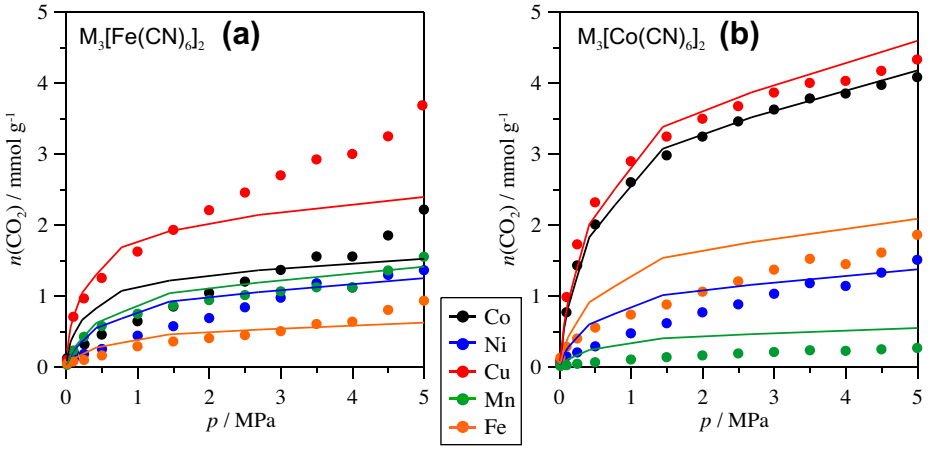

Fig. 3. Comparison between experimental and predicted (Monte Carlo simulations) adsorption isotherms at 318 K for the studied Prussian blue analogues. Symbols: filled circles show experimental data, and lines predicted data.

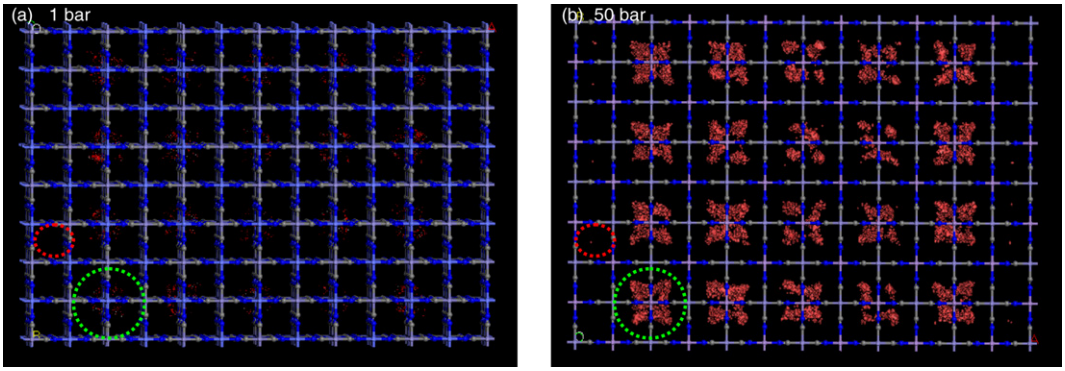

Fig. 4. Calculated isodensity surfaces (red surfaces) for CO_2 molecules in $[Mn_3Fe_2]$ at 318 K and (a) 1 and (b) 50 bar. Red and green dashed lines show CO_2 distribution in small and large pores, respectively.

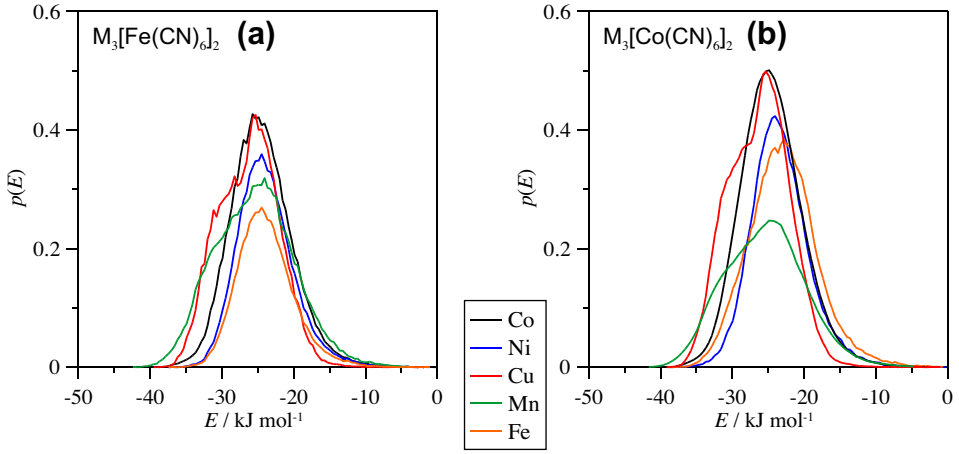

Fig. 5. Probability distribution functions, $P(E)$, for CO_2-sorbent interaction energies at 318 K and 50 bar.

distances follow the ordering M^{III}=Co < Cu < Ni < Mn < Fe. Therefore, although the relationship between CO_2 adsorption ability and M^{III}–C bond distance is not straightforward, the results point to the fact that the shorter the M^{III}–C bond distance the larger the CO_2 capturing capacity, especially for compounds containing M^{II}=Co and Cu. On the other side, the relationship between the 'accessible area/free volume' and the CO_2 adsorption ability is not clear. Although larger accessible areas and free volumes should contribute to increase capturing ability, in fact compounds with lower values of these properties, such as those containing M^{II}=Cu and Co (both for $M_3[Fe(CN)_6]_2$ and $M_3[Co(CN)_6]_2$), lead to the larger CO_2 adsorption (Fig. 3). Therefore, considering the moderate differences between the accessible areas and free volumes between the studied compounds, Table 3, the main factor controlling the CO_2 adsorption ability seem to rise from the characteristics (ionicity) of the M^{III}–C and M^{II}–N bonds. Nevertheless, differences between these properties for the studied compounds are very subtle and cannot be systematized in a simple manner.

In order to analyze the affinity between the CO_2 molecules and the corresponding sorbents, we have calculated from Monte Carlo simulations the distribution functions of CO_2-sorbent interaction energies, Fig. 5. The values reported in Fig. 5 are in agreement with CO_2 adsorption ability, both for $[M_3Fe_2]$ and $[M_3Co_2]$ compounds, the stronger the interaction energies the larger the adsorption.

For PB analogues containing M^{II}=Cu and Co (compounds with the larger CO_2 adsorption), $p(E)$ curves show stronger peaks, and in the case of $[Cu_3Fe_2]$ and $[Cu_3Co_2]$, interaction energies extend to regions in the −30 to −35 kJ mol^{-1}, whereas for most of the sorbents peaks around −25 kJ appear, which could justify the larger adsorption ability of Cu-based PB analogues. Therefore, the CO_2-sorbent affinity measured through the results reported in Fig. 5a is closely related with CO_2 absorption ability for the studied compounds. The variation of CO_2-sorbent energy with pressure is analyzed in Fig. 4 for $[Mn_3Fe_2]$ (although analogous results are inferred for the remaining sorbents). As the pressure increases interaction

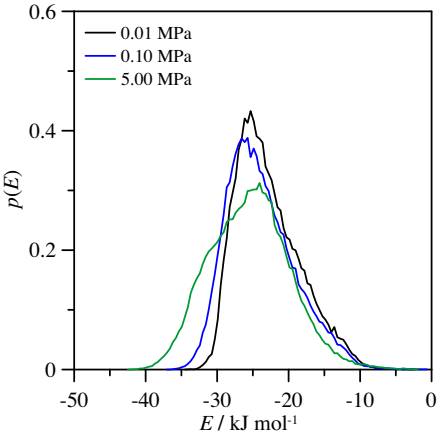

Fig. 6. Probability distribution functions, $P(E)$, for CO_2-sorbent interaction energies for $[Mn_3Fe_2]$ at 318 K and variable pressure.

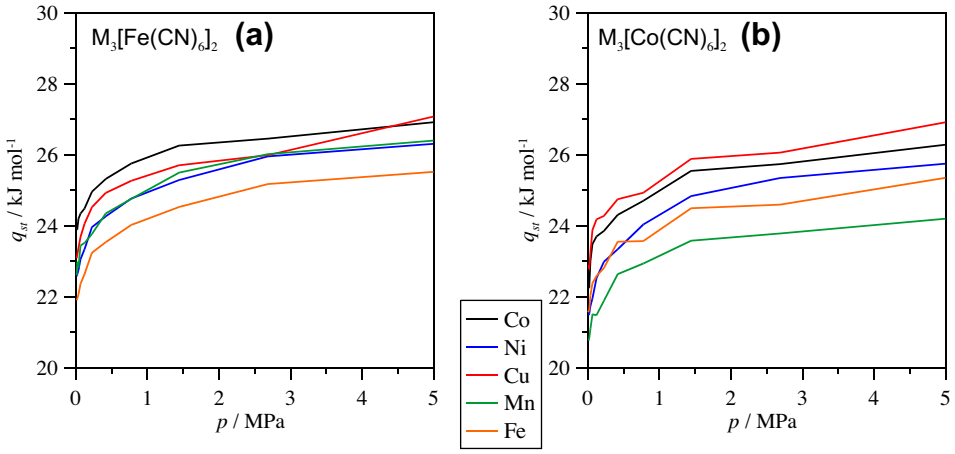

Fig. 7. Isosteric heat of adsorption, qst, obtained from Monte Carlo simulations at 318 K for CO_2 in the studied PB sorbents.

energies shift toward higher values (in absolute value), which through comparison with results reported in Fig. 4 should correspond to the adsorption in small pores, in which CO_2 and sorbent framework interact strongly. Therefore, energy distribution functions also show that small pores are occupied for high pressures, whereas for low and intermediate pressures large pores seem to be occupied.

Finally, we have also calculated the isosteric heat of adsorption, q_{st}, in the seven studied PB sorbents, Fig. 6. The q_{st} values follow the same trend as the CO_2 sorption ability reported in Fig. 3: the higher the q_{st}, the higher the CO_2 sorption. The changes of q_{st} with pressure follow the same trend for all the studied PB analogues: increases around 2 kJ mol^{-1} from low pressure (low loadings) to around 15 bar, and then it remains almost constant for higher pressures. This may be related with the occupancy of large pores for low pressures, corresponding to weaker CO_2-sorbent interactions, and then with increasing pressures increasing concentration in small pores, with stronger CO_2-sorbent interaction, and thus, larger q_{st}. Nevertheless, considering the low occupancy of small pores, as reported in Fig. 4, q_{st} does not change remarkably once the large pores are occupied. (See Fig. 7).

4. Conclusion

A collection of ten Prussian blue analogues, corresponding to M′[M(CN)$_6$], have been prepared and characterized to study their CO_2 capture capacities up to 50 bar. The ions M′ and M were changed in a systematic manner to infer their effect on Prussian blue analogues structural properties and on their CO_2 adsorption capacities. CO_2 isothermal adsorption measurements were carried out using a state-of-the-art magnetic suspension balance. This is the first high pressure CO_2 adsorption study on Prussian blue type compounds available in the literature in which measurements were extended in the high pressure range (up to 50 bar).

All the studied compounds show *Fm3m* crystal structure with crystal vacant position occupied with guest water molecules in different amounts. Water molecules can be eliminated through heating without disrupting the crystal structure, and thus, leaving holes available for CO_2 molecules. The highest CO_2 adsorption in M′[M(CN)$_6$] compounds is obtained when M′=Cu both for M=Fe and Co, with values 2–4 times those of the remaining Prussian blue analogues.

Grand canonical Monte Carlo simulations leaded to predicted CO_2 adsorption isotherms in good agreement, both qualitative and quantitative, with experimental results. From a nanoscopic viewpoint, the simulation results show the preferential CO_2 adsorption in large cavities for low to moderate pressures, whereas small cavities are occupied only in the high pressure range. The analysis of available free volume showed very small differences between in the studied compounds, which are not related with the adsorption ability. Likewise, the analysis of M^{III}–C and M^{II}–N distances leaded to the conclusion of the larger M^{III}–C bond distance, the larger the CO_2 capturing capacity. Nevertheless, the main factor controlling the adsorption ability of the studied Prussian blue analogues, considering the small differences in free volumes and interatomic distances, is the CO_2 – sorbent affinity; the larger the interaction energy, the larger the adsorption ability. Therefore Cu containing compounds show the larger interaction energies, and thus, the larger CO_2 adsorption capacities.

CO_2 adsorption isotherms show sudden changes in the 35–40 bar range for all the studied compounds, this interesting effect remained occult in previous available literature works, which were limited to lower pressures. Work is in progress to better understand this behavior.

Acknowledgement

This paper was made possible by the support of an NPRP grant (No. NPRP-08-670-1-124) from The Qatar National Research Fund. The statements made herein are solely the responsibility of the authors.

Appendix A. Supplementary data

Supplementary data associated with this article can be found, in the online version, at http://dx.doi.org/10.1016/j.micromeso.2012.06.019.

References

[1] K.R. Dunbar, R.A. Heintz, Prog. Inorg. Chem. 45 (1997) 283–291.
[2] J. Lee, O.K. Farha, J. Roberts, A.K. Scheidt, S.T. Nguyen, J.T. Hupp, Chem. Soc. Rev. 38 (2009) 1450–1459.
[3] Y.S. Bae, O.K. Farha, J.T. Hupp, R.Q. Snurr, J. Mater. Chem. 19 (2009) 2131–2134.
[4] M.R. Kishan, P.K. Thallapally, J. Tian, C.A. Fernandez, S.J. Dalgarno, J.E. Warren, J.L. Atwood, B.P. McGrail, Chem. Comm. (2010) 538–540.
[5] A.A. Karyakin, Electroanalysis 13 (2001) 813–819.
[6] N. De Taconi, K. Rajeshwar, R.O. Lezna, Chem. Mater. 15 (2003) 3046–3062.
[7] C.D. Wu, A. Hu, L. Zhang, W. Lin, J. Am. Chem. Soc. 127 (2005) 8940–8941.
[8] P.K. Thallapally, J. Tian, M.R. Kishan, C.A. Fernandez, S.J. Dalgarno, P.B. McGrail, J.E. Warren, J.L. Atwood, J. Am. Chem. Soc. 130 (2008) 16842–16843.
[9] E. Ruiz, A. Rodriguez-Fortea, S. Alvarez, M. Verdaguer, Chem. Eur. J. 11 (2005) 2135–2144.
[10] S.S. Kaye, J.R. Long, J. Am. Chem. Soc. 127 (2005) 6506–6507.
[11] P.K. Thallapally, R.K. Motkuri, C.A. Fernandez, B.P. McGrail, G.S. Behrooz, Inorg. Chem. 49 (2010) 4909–4915.

[12] F. Karadas, C.T. Yavuz, S. Zulfiqar, S. Aparicio, G.D. Stucky, M. Atilhan, Langmuir 27 (2011) 10642–10647.
[13] S. Natesakhawat, J.T. Culp, C. Matranga, B. Bockrath, J. Phys. Chem. C 111 (2007) 1055–1060.
[14] J. Jiménez-Gallegos, J. Rodríguez-Hernández, H. Yee-Madeira, E. Reguera, J. Phys. Chem. C 114 (2010) 5043–5048.
[15] A.K. Rappe, C.J. Casewit, K.S. Colwell, W.A. Goddard, W.M. Skiff, J. Am. Chem. Soc. 114 (1992) 10024–10035.
[16] A.K. Rappe, W.A. Goddard, J. Phys. Chem. 95 (1991) 3358–3363.
[17] Materials Studio 5.5; Accelrys Inc.: San Diego, CA, 2010.
[18] J.J. Potoff, J.I. Siepmann, AIChE J. 47 (2001) 1676–1682.
[19] K. Itaya, I. Uchida, Acc. Chem. Res. 19 (1986) 162–168.
[20] T. Düren, F. Millange, G. Ferey, K.S. Walton, R.Q. Snurr, J. Phys. Chem. C 111 (2007) 15350–15356.
[21] Q. Yang, C. Zhong, J.F. Chen, J. Phys. Chem. C 112 (2008) 1562–1569.
[22] P. He, H. Liu, Y. Li, Z. Lei, S. Huang, P. Wang, H. Tian, Mol. Sim. 38 (2012) 72–83.
[23] M.V. Bennett, L.G. Beauvais, M.P. Shores, J.R. Long, J. Am. Chem. Soc. 123 (2001) 8022–8032.
[24] A. Bleuzen, J.D. Cafun, A. Bachschmidt, M. Verdaguer, P. Munsch, F. Baudelet, J.P. Itie, J. Phys. Chem. C 112 (2008) 17709–17715.
[25] S. Margadonna, K. Prassides, A.N. Fitch, J. Am. Chem. Soc. 126 (2004) 15390–15391.
[26] P.K. Thallapally, R.K. Motkuri, C.A. Fernandez, P. McGrail, G.S. Behrooz, Inorg. Chem. 49 (2010) 4909–4915.
[27] R.K. Motkuri, P.K. Thallapally, O.P. McGrail, S.B. Ghorishi, Cryst. Eng. Comm. 12 (2010) 4003–4006.
[28] A.O. Yazaydin, R.Q. Snurr, T.H. Park, K. Koh, J. Liu, M.D. LeVan, A.I. Benin, P. Jakubczak, M. Lanuza, D.B. Galloway, J.J. Low, R.R. Willis, J. Am. Chem. Soc. 131 (2009) 18198–18199.